

The planar pyrochlore: a Valence Bond Crystal.

J.-B. Fouet, M. Mambrini, P. Sindzingre, C. Lhuillier

Laboratoire de Physique Théorique des Liquides-UMR 7600 of CNRS, Université Pierre et Marie Curie, case 121, 4 place Jussieu, 75252 Paris Cedex, France
E-mail:fouet@lptl.jussieu.fr

(October 24, 2018)

Exact diagonalizations of the spin-1/2 Heisenberg model on the checkerboard lattice have been performed for sizes up to $N = 36$ in the full Hilbert space and $N = 40$ in the restricted subspace of first neighbor dimers. This antiferromagnet does not break $SU(2)$ symmetry and displays long range order in 4-spin $S=0$ plaquettes. Both the symmetry properties of the spectrum and various correlations functions are extensively studied. At variance with the kagomé antiferromagnet, the Heisenberg quantum model on a checkerboard lattice is a Valence Bond Crystal. Some results concerning the 3-dimensional spin-1/2 pyrochlore magnet (for sizes 16 and 32) are also shown: this system could behave differently from its 2-dimensional analog.

PACS numbers: 75.10.Jm; 75.50.Ee; 75.40.-s

I. INTRODUCTION

In the family of frustrated magnets, the kagomé and pyrochlore lattices have attracted special attention both experimentally and theoretically. Experimentally such magnets display a wide variety of unusual low temperature behaviors [1–6] signatures of different kind of collective low energy degrees of freedom.

The first-neighbor classical Heisenberg model on such lattices has a $T=0$ entropy [7]. On these lattices, the Heisenberg model can be rewritten as the sum of the square of the total spin of corner sharing units α (triangles for the kagomé lattice, tetrahedra in the pyrochlore):

$$\mathcal{H} = J \sum_{(i,j) \text{ bonds}} \mathbf{S}_i \cdot \mathbf{S}_j \equiv \frac{J}{2} \sum_{\alpha \text{ units}} \mathbf{S}_\alpha^2 + Cst. \quad (1.1)$$

Thus a classical ground-state is obtained whenever $\mathbf{S}_\alpha = 0$ for all α . It is a straightforward exercise to show that such ground-states have a continuous local degeneracy. Thermal fluctuations select planar spin configurations on the kagomé lattice [8,9], but are unable to build order from disorder in the pyrochlore lattice [10].

A simple Maxwellian counting has been done by the last authors: the number of degrees of freedom of N Heisenberg spins with a given length is $F = 2N$. The number of constraints to realize a classical ground-state is $K = 6N/q$ where q is the number of spins on each α unit. Assuming that these constraints are linearly indepen-

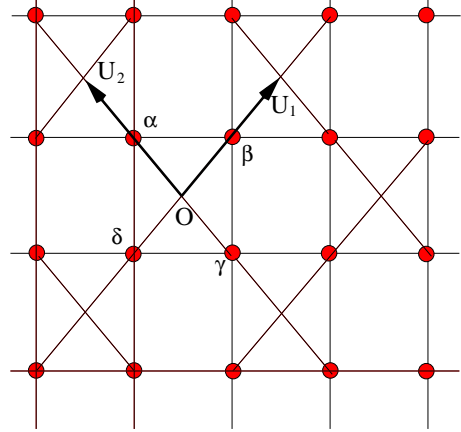


FIG. 1. The checkerboard lattice: the spins sit at the vertices shown by bullets, all couplings are identical, $\mathbf{u}_1, \mathbf{u}_2$ are the unit vectors of the Bravais lattice.

dent¹, one finds a $T = 0$ extensive entropy ($F - K \sim N$) for the pyrochlore and zero entropy ($F - K \sim 0$) in the kagomé case. Although the assumption is known to fail for the kagomé magnet this naive counting suggests that the degeneracy of the classical ground-state in the pyrochlore magnet is larger than in kagomé magnet, in qualitative agreement with the thermal behavior of the two magnets.

Lately, Palmer and Chalker have studied the Heisenberg problem on the checker-board lattice [11]. This lattice built out of corner sharing 4-spin squares (see Fig. 1) is the two dimensional analog of the pyrochlore lattice. The classical Heisenberg model on the checker-board lattice has a similar ground-state degeneracy and behave the same way at low temperature (and with additional dipolar interactions) [11].

The effect of quantum fluctuations on these different structures remains to be fully understood. In the large S , first-order spin-wave approximation, all these magnets remain disordered [12]. Higher order approximations have been devised for the kagomé lattice and lead to selection of order out of disorder by quantum fluctuations [13]. There is no spin long range order (LRO) in the pyrochlore magnet [14,15].

The spectrum of low lying excitations of the spin-

¹This has been argued to be true in the pyrochlore case [10].

1/2 kagomé magnet obtained from exact diagonalizations has been a real surprise [16,17]: whereas it probably has a small gap for $\Delta S = 1$ excitations (transitions $S = 0 \rightarrow S = 1$), there is no gap to singlet excitations (transitions $S = 0 \rightarrow S = 0$) and the density of low lying $S = 0$ states is so large that the system has a $T=0$ residual entropy. The discovery of a second model with a similar spectrum of low lying excitations on the triangular lattice with 4-spin exchange interaction lead us to speculate that this could be a generic new type of magnets [18,19]. A natural question thus arises: do the 2-dimensional and the true pyrochlore quantum magnets belong to this generic class? The results obtained from their classical and semi-classical counterparts support the speculation that the answer might be positive! As exact diagonalizations are up to now limited to systems of $N \sim 36$ spins, the problem of the true spin-1/2 pyrochlore magnet might remain open for still a long time. The 2-d pyrochlore looks more promising: Palmer and Chalker [20] have computed the spectra of clusters up to 24 spins. From their results, they were able to conclude that the system has no Néel LRO; it does not break $SU(2)$ at $T = 0$ and probably has a large spin gap. Yet these sizes were not large enough to be sure that this magnet was really in the same class as the kagomé magnet. In this work we extend such diagonalizations up to $N = 36$. The technical aspects of these diagonalizations have been previously described [21].

Besides these diagonalizations in the full Hilbert space, we also have performed diagonalizations in the restricted space of first neighbor dimer coverings (denoted in the following FNSS, for First Neighbor Singlet Subspace). The size of this restricted subspace is smaller than the $S = 0$ sector of the full Hilbert space and it increases slower with the system size ($\sim 1.33^N$ compared to $\sim 2^N$). In this restricted basis we have studied samples up to $N = 40$. The FNSS calculations for $N = 40$ have required an order of magnitude less of computer memory than the full Hilbert space calculations for $N = 36$. As usual, periodic boundary conditions are applied to the samples.

II. ENERGY PER SPIN OF THE GROUND-STATE IN THE FULL HILBERT SPACE

The absolute ground-state is an $S=0$ state [22], in the trivial representation of the space group. The ground-state energy per spin versus system size is given in Fig. 3 and in Table I. The samples are displayed in Fig. 2. Our results are identical to those of Palmer and Chalker [20] for the small sizes and identical shapes. We have added some extra shapes (indexed by a prime) to show the sensitivity of small size results to the shape. The analysis of the whole set of results shows that the most stable small samples largely overestimate the thermodynamic binding energy. In fact the first three samples 16, 20, 24 can be

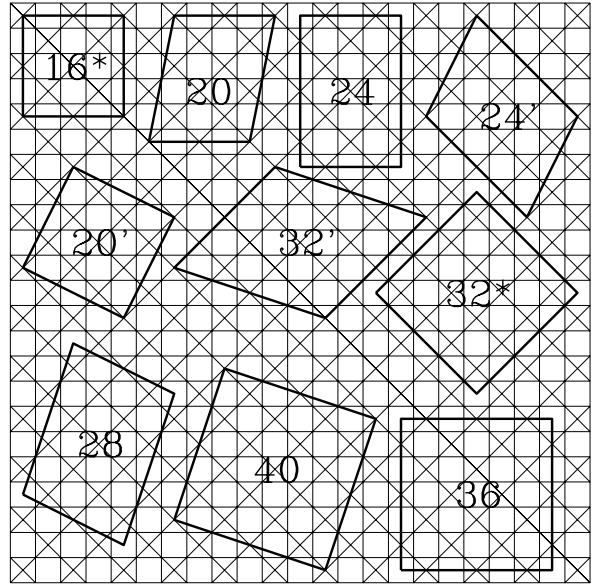


FIG. 2. Samples: the star indicates that the sample has extra symmetries not shared by the checkerboard infinite lattice (see text), the prime indicates that the sample has higher ground-state energy than the other with the same number of spins.

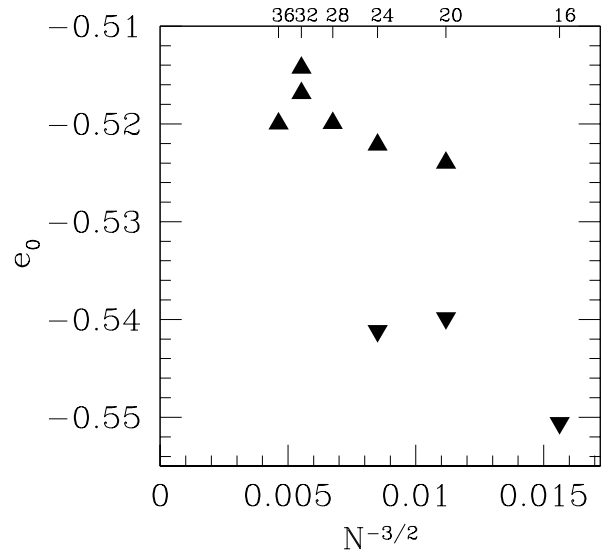


FIG. 3. Energy per spin e_0 vs $N^{-3/2}$ for “true 2-dimensional samples” (full upwards triangles) and “quasi 1-dimensional tubes” (downwards triangles) (see text).

N	16*	20	24	24'	28	32*	32'	36
e_0	-0.551	-0.540	-0.541	-0.522	-0.520	-0.517	-0.514	-0.520
$E_{S=1}^1 - E_{S=0}^1$	1.12	0.96	1.00	0.58	0.57	0.69	0.57	0.71
$E_{S=0}^2 - E_{S=0}^1$	0.37	0.30	0.20	0.08	0.09	0.03	0.01	0.05
$E_{S=0}^3 - E_{S=0}^2$.53	0.22	0.28	0.06	0.05	0.18	0.13	0.22
$E_{S=1}^1 - E_{S=0}^3$	0.23	0.44	0.52	0.44	0.42	0.47	0.43	0.44
n_1	27	25	38	51	82	286	135	110
$\ln(n_1)/N$	0.21	0.16	0.15	0.16	0.16	0.18	0.15	0.13

TABLE I. Spectrum of the Heisenberg model in the full Hilbert space. Energy per spin in the ground-state e_0 and energy gaps $E_S^{n_S} - E_{S'}^{n_{S'}}$ between the n_S energy level of the S' spin sector and the n_S level of the S sector. Second line: spin gap. Third line: gap between the absolute ground-state and the first singlet excitation. Fourth line: gap between the second and third level in the $S = 0$ sector. Fifth line: gap between the third level in the $S = 0$ sector and the first triplet excitation. Following lines: n_1 is the number of singlet states in the spin gap (including degeneracies). The starred columns correspond to samples which have the extra symmetries of the pyrochlore lattice. The three first columns are 4-spins tubes.

seen as tubes with a 4-spin section. The properties of these quasi 1-dimensional systems is different from those of the true 2-dimensional samples (see section VI). This is manifest in Fig.3 and following and has also been checked on the properties of the ground-state wave-function.

The energy per spin for the largest sizes seems to level off in the range $[-0.52, -0.51]$.

The still non negligible size effect found on samples 28, 32 and 36 has to be related to symmetry problems: the 28 sample has not all the symmetries of the infinite lattice and the 32* sample (as the 16* sites sample) has extra symmetries not shared by the checkerboard infinite lattice (see below). So in all respects the 36 sample seems the better sample to mimic the checkerboard infinite lattice: its energy gives a plausible lower bound of the thermodynamic limit².

Samples 16* and 32* are peculiar. There is in fact a one to one mapping, preserving neighborhood relationships and periodic boundary conditions, between these samples on the checkerboard lattice and the cells of the same size of a pyrochlore. Their symmetry group has extra symmetries inherited from those of the pyrochlore lattice. This explains the extra degeneracy noticed on exact spectra of these "pyrochlore" samples, when analyzed with the checkerboard symmetry group³.

²Its only weakness could be the absence of fluctuations at wave-vectors $(0, \pi), (\pi, 0)$, but all the information gathered on this system lead us to conclude that this absence is not qualitatively essential.

³Numerical results available on request at

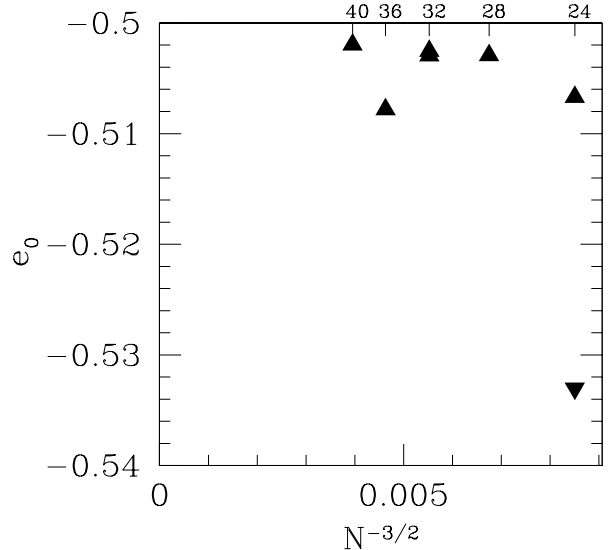


FIG. 4. Energy per spin in the FNSS subspace. Symbols are the same as in Fig. 3. The two $N = 32$ results are nearly indistinguishable with the scale of the symbols.

N	24	24'	28	32*	32'	36	40
$E_{S=0}^2 - E_{S=0}^1$	0.340	0.080	0.035	0.025	0.027	0.050	0.014
$E_{S=0}^3 - E_{S=0}^2$	0.47	0.35	0.31	0.45	0.44	0.49	0.45
$(E_{var} - E_{ex})/E_{ex}$	0.015	0.029	0.008	0.027	0.023	0.023	

TABLE II. Spectrum of the Heisenberg Hamiltonian in the first neighbor singlet subspace. First two lines: energy gaps in the singlet sector (same definitions as in Table 1). Last line: relative difference in ground-state energy between the FNSS and the full Hilbert space.

III. GROUND-STATE IN THE FIRST-NEIGHBOR DIMER SUBSPACE

Results of diagonalizations in the first neighbor singlet subspace (Fig. 4 and Table II) confirm the above-mentioned hypotheses and call for the following comments:

- The variational energy in the FNSS is $\sim 2\%$ above the exact one. This property is not spoiled by increasing system size. We might thus expect that this variational subspace capture most of the physics of the exact ground-state.
- The size and shape effects on the $S = 0$ ground-state are roughly the same in the two sets of results.

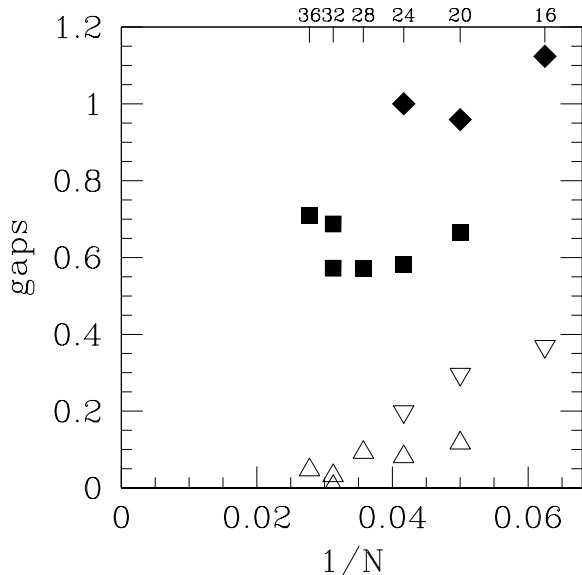


FIG. 5. Full Hilbert space: energy gaps measured from the absolute ground-state versus $1/N$. Full squares (diamonds): spin-gaps for 2-dimensional samples (4-spin tubes). Open triangles pointing up (down): gaps to the 2^{nd} singlet energy level for 2-dimensional samples (4-spin tubes).

Due to the partial cut-off of long dimers the size effects in the FNSS are smaller than in the exact ground-state.

- The anomaly of the $N=32$ sample is less pronounced in the FNSS. This can be understood as this basis does not allow expression of the full ternary symmetry of the 3d pyrochlore. In fact the difference in ground-state energy between the two different 32 samples is hardly visible on the scale of Fig. 4.
- The 40 sites sample has an energy in the same range as the $N=28,32,36$ samples confirming that the larger sizes are in a cross-over regime, with linear dimensions of the order of, or larger than the spin-spin correlation length.

IV. SPIN GAP

The spin gap (defined as the difference in total energy between the first $S = 1$ excited state and the $S = 0$ absolute ground-state) is displayed in Fig. 5 and Table I (line 2) versus system size, and in Fig. 6 versus ground-state energy per spin. This last figure emphasizes the difference between the quasi 1-dimensional systems (tubes) with a large binding energy (~ -0.54) and a large gap (~ 1), and the true 2d systems with a binding energy (~ -0.52) and a gap of the order of 0.6 times the coupling constant.

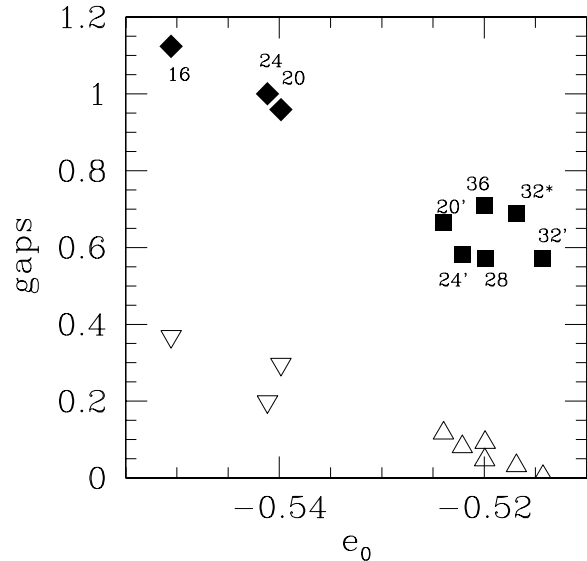


FIG. 6. Full Hilbert space: correlations between gaps and ground-state energy per site. Same symbols as in Fig. 5.

V. SPECTRUM OF THE FIRST EXCITATIONS IN THE $S = 0$ SECTOR

The first excited state in the full singlet sector collapses to the ground-state with increasing system size (third line of Table 1, open triangles in Figs. 5 and 6). The same phenomenon is clearly seen in the FNSS (Table 2 and Fig. 7). This is a clear indication of a degeneracy of the absolute ground-state in the thermodynamic limit. In this system with two spins $1/2$ per unit cell we do not expect a topological degeneracy [23]. We will explicit in the next section the space symmetry breaking at the origin of the present degeneracy.

Analysis of the gap between the second and third singlet (fourth line of Table 1 in the full Hilbert space, 2nd line of Table 2 in the FNSS and Fig. 7) shows a non monotonous behavior and no tendency to close for larger sizes. On the basis of the present results one expects, in the thermodynamic limit, a finite gap in the singlet sector above the 2-fold degenerate ground-state and this gap is probably smaller than the gap to the first triplet (fifth line of Table 1 to be compared to the second line of this same table).

Also shown in Table 1 is the number n_1 of singlet states in the spin-gap. The unusually large values of n_1 found for the small samples were taken by Palmer and Chalker [20] as indications of a similarity of the checkerboard and the kagomé magnet. These large values are probably an indication of a continuum of singlet excitations. But this continuum appear to be separated from the ground-state by a finite gap. So the continuous density of singlet states adjacent to the ground-state, that is the distinctive

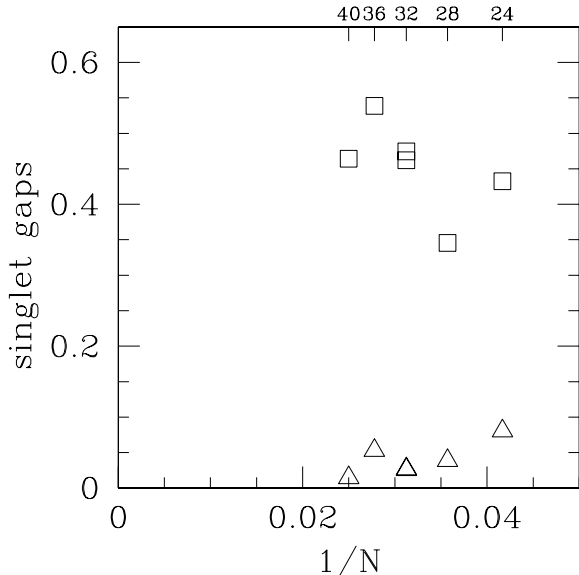


FIG. 7. Gaps in the singlet sector. Open triangles (open squares): gap from the ground-state to the first (second) excited state in the FNSS.

characteristic of the kagomé magnet, is absent in the 2-dimensional checkerboard lattice (Fig. 7).

Endly the continuum of singlet excitations above the third level of the true checker-board spectra can be interpreted as the excitations of antiferromagnetic pairs of confined spinons. The ferromagnetic pairs appear more energetic (fifth line of Table 1 to be compared to the second line).

In view of the results for the $N = 16^*$ and 32^* “pyrochlore” samples one might speculate a different behavior for the pyrochlore lattice: n_1 is indeed much larger than for other sizes (Table. I). But no continuum is yet actually visible in the spectrum as it is in the kagomé spectrum. There is still a noticeable gap between the second and third singlet eigenlevels in the 32^* sample. Larger sizes would be necessary to really see if the pyrochlore belongs to the same generic class as the kagomé.

VI. GROUND-STATE SYMMETRY BREAKING

As noticed above the finite size results point to a 2-fold degeneracy of the ground-state in the thermodynamic limit. The absolute ground-state is in the trivial representation of the lattice symmetry group. Its wave function is invariant in any translation and in any operation of D_4 : group of the $\pi/2$ rotations around point O (or any equivalent point of the Bravais lattice) and axial symmetries with respect to axes \mathbf{u}_1 and \mathbf{u}_2 (see Fig. 1). The excited state which collapses on it in the thermodynamic limit has a wave vector (π, π) (its wave function takes a (-1) factor in one-step translations along \mathbf{u}_1 or \mathbf{u}_2), and it

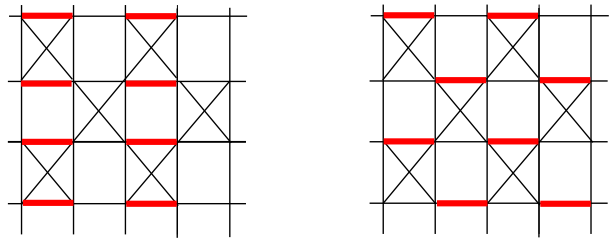


FIG. 8. Columnar and staggered configuration of dimers (fat links) on the checkerboard lattice: such symmetry breaking configurations are 4-fold degenerate in the thermodynamic limit.

is odd under $\pi/2$ rotations and axial symmetries. In the thermodynamic limit the 2-fold degenerate ground-state can thus exhibit a spontaneous symmetry breaking with a doubling of the unit cell. Such a restricted symmetry breaking does not allow a columnar or staggered configuration of dimers (Fig. 8): both of these states have at least a 4-fold degeneracy.

The simplest Valence Bond Crystals that allow the above-mentioned symmetry breaking are described by pure product wave-functions of 4-spin $S=0$ plaquettes. This family includes eight different configurations:

- The singlet plaquettes may sit either on the squares with crossed links or on the void squares (A and B configurations of Fig. 9),
- The translation symmetry breaking configurations may be in two different locations named $A_{1(2)}$ (resp $B_{1(2)}$),
- An $S=0$ state on a plaquette of four spins sitting on sites $(\alpha, \beta, \gamma, \delta)$ may be realized either by the symmetric combination of pairs of singlets:

$$|\psi^+\rangle = |\alpha \rightarrow \delta\rangle |\gamma \rightarrow \beta\rangle + |\alpha \rightarrow \beta\rangle |\gamma \rightarrow \delta\rangle, \quad (6.1)$$

or by the anti-symmetric one:

$$|\psi^-\rangle = |\alpha \rightarrow \delta\rangle |\gamma \rightarrow \beta\rangle - |\alpha \rightarrow \beta\rangle |\gamma \rightarrow \delta\rangle. \quad (6.2)$$

where $|\alpha \rightarrow \gamma\rangle$ is the singlet state on sites α and γ :

$$|\alpha \rightarrow \gamma\rangle = (|\alpha \uparrow, \gamma \downarrow\rangle - |\alpha \downarrow, \gamma \uparrow\rangle) / \sqrt{2}. \quad (6.3)$$

We can thus define eight different product wave-functions labeled: $|A_{1(2)}^\epsilon\rangle$ and $|B_{1(2)}^\epsilon\rangle$. The transformations of these states under the elementary operations of the lattice symmetry group are described in the first four lines of Table III. The symmetric (resp. anti-symmetric) linear combinations of these states which are irreducible representations of this group are defined in

Wave-function	$\mathcal{T}_{\mathbf{u}_1}$	$\mathcal{R}_{\pi/2}$	$\sigma_{\mathbf{u}_1}$
$A_{1(2)}^+$	$A_{2(1)}^+$	$A_{1(2)}^+$	$A_{1(2)}^+$
$A_{1(2)}^-$	$A_{2(1)}^-$	$(-1)^p A_{1(2)}^-$	$(-1)^p A_{1(2)}^-$
$B_{1(2)}^+$	$B_{2(1)}^+$	$B_{2(1)}^+$	$B_{2(1)}^+$
$B_{1(2)}^-$	$B_{2(1)}^-$	$(-1)^p B_{2(1)}^-$	$(-1)^p B_{2(1)}^-$
$X^\eta = A_1^+ + \eta A_2^+$	ηX^η	X^η	X^η
$Y^\eta = A_1^- + \eta A_2^-$	ηY^η	$(-1)^p Y^\eta$	$(-1)^p Y^\eta$
$Z^\eta = B_1^+ + \eta B_2^+$	ηZ^η	ηZ^η	ηZ^η
$T^\eta = B_1^- + \eta B_2^-$	ηT^η	$(-1)^p \eta T^\eta$	$(-1)^p \eta T^\eta$

TABLE III. Transformation rules of the product wave-functions in the elementary operations of the symmetry group (the space group is defined with respect to point O and translations $\mathbf{u}_1, \mathbf{u}_2$). The wave-functions of the anti-symmetric plaquettes have different symmetries depending on the parity p of the number of plaquettes in the sample.

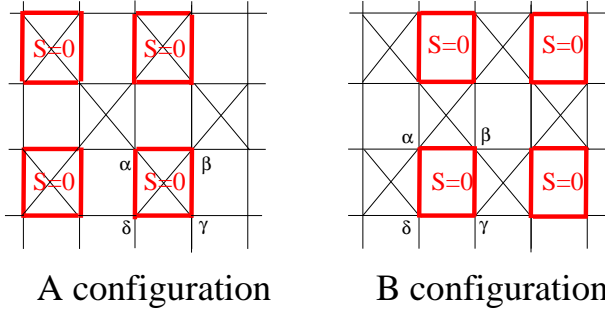


FIG. 9. $S=0$ 4-spin plaquette valence-bond crystals on the checkerboard lattice: fat links indicate 4 spins involved in a singlet.

the four last lines of the same Table. The comparison of the symmetries of these states with those of the two first levels of the exact spectra indicates a Z type symmetry of the checker-board magnet ground-state: in the thermodynamic limit the symmetry breaking configuration is thus of the B type decorated by the symmetric 4-spin plaquettes described in Eq.6.1 (anti-symmetric 4-spin plaquettes are excluded by the properties of the exact ground-state and first singlet excitation in samples with an odd number of 4-spin plaquettes, such as $N=28$ or 36).

Indeed in the exact ground-state quantum fluctuations might dress the product states giving a more fuzzy picture. Insofar as gaps to the third singlet state and the first triplet remain finite in the thermodynamic limit, the Valence Bond Crystal picture (with LRO in plaquettes) will survive to quantum fluctuations.

A simple last remark could be done: the symmetric-plaquette state (Eq. 6.1) can be rewritten as the product of two triplets along the diagonals of the square. This configuration of spins is not energetically optimal on the

i, j	ex. g.-s.	Z w-f.	FNSS	i, j	ex. g.-s.	Z w-f.
1,2	-0.239	-0.25	-0.27	1,29	0.001	0.
1,8	-0.043	0.	0.033	1,17	-0.002	0.
1,32	0.088	0.125	0.122	1,4	-0.037	0.
1,3	0.034	0.		1,10	-0.012	0.
1,35	0.013	0.	-0.018	1,16	-0.001	0.

TABLE IV. Spin-Spin correlations $\mathcal{C}^2(i, j) = \langle \mathbf{S}_i \cdot \mathbf{S}_j \rangle$ in the exact ground-state (second columns), in the variational Z wave-function (third columns), and in the ground-state of the first neighbor singlet subspace (fourth columns) of the $N=36$ sample. The sites i, j are numbered as in Fig. 10.

squares with antiferromagnetic crossed links (A configuration) but might a priori be favored in B configuration. Reversely the ψ^- -plaquette can be rewritten as the product of two singlets along the diagonals of the square, and would eventually be preferred in A configuration. The variational energy per spin of the product wave-function of ψ^+ plaquettes in B configuration is $E_{var}(B^+) = -0.5$, whereas the variational energy per spin of the product wave-function of ψ^- plaquettes in A configuration is $E_{var}(A^-) = -0.375$. For the quasi 1-dimensional samples 16,20 and 24, these symmetric plaquettes can be built not only on square voids but also along the 4-spin cross section of the tube. The resonance between plaquettes on void square and plaquettes on the cross section might explain the special properties (energy, gaps, correlations) of these samples.

Exact results are indeed consistent with this variational estimate and favor ψ^+ -plaquettes on voids. This is in agreement with recent results of Moessner *et al* [24] but is at variance with the departure point of the strong coupling approximation of Elhajal *et al* [25].

VII. CORRELATIONS

As it was expected for a Valence Bond Crystal it can be seen in Table IV that spin-spin correlations in the $N = 36$ exact ground-state decrease very rapidly with distance. The decrease with distance is even more rapid in the full Hilbert space than in the FNSS. In this respect the Z product wave-function appears to be a good simple variational guess to describe the exact ground-state.

The 4-point correlation function:

$$\mathcal{C}^4(1, 2; i, j) = 4 [\langle \mathbf{S}_1 \cdot \mathbf{S}_2 \mathbf{S}_i \cdot \mathbf{S}_j \rangle - \langle \mathbf{S}_1 \cdot \mathbf{S}_2 \rangle \langle \mathbf{S}_i \cdot \mathbf{S}_j \rangle] \quad (7.1)$$

is displayed in Table V in the exact ground-state, in the Z product wave-function and in the ground-state of the First Neighbor Singlet Subspace (see also Fig. 10). Here again the general behaviors are quite similar. As it was expected quantum fluctuations in the exact g.-s. renormalize the correlations at intermediate and larger

distances. Asymptotic behavior seems approximately reached for the larger distances in sample $N = 36$. Renormalization by quantum fluctuations amounts to $\sim 60\%$ of the bare variational Z value.

Due to the plaquette structure of this Valence Bond Crystal a better order parameter is given by the cyclic permutation operator $P_{\alpha,\beta,\gamma,\delta}$ of the 4 spins $(\alpha, \beta, \gamma, \delta)$ on the square plaquette. Let us define the corresponding hermitic observable as:

$$\begin{aligned} Q_{\alpha,\beta,\gamma,\delta} &= \frac{1}{2}(P_{\alpha,\beta,\gamma,\delta} + P_{\alpha,\beta,\gamma,\delta}^{-1}) \\ &= 2[\mathbf{S}_\alpha \cdot \mathbf{S}_\beta \mathbf{S}_\gamma \cdot \mathbf{S}_\delta + \mathbf{S}_\alpha \cdot \mathbf{S}_\delta \mathbf{S}_\beta \cdot \mathbf{S}_\gamma - \mathbf{S}_\alpha \cdot \mathbf{S}_\gamma \mathbf{S}_\beta \cdot \mathbf{S}_\delta] \\ &\quad + 0.5[\mathbf{S}_\alpha \cdot \mathbf{S}_\beta + \mathbf{S}_\gamma \cdot \mathbf{S}_\delta + \mathbf{S}_\alpha \cdot \mathbf{S}_\delta + \mathbf{S}_\beta \cdot \mathbf{S}_\gamma] \\ &\quad + 0.5[\mathbf{S}_\alpha \cdot \mathbf{S}_\gamma + \mathbf{S}_\beta \cdot \mathbf{S}_\delta + 1/4] \end{aligned} \quad (7.2)$$

Its value in the $N=36$ exact ground-state (resp. in the Z variational w.-f.) is 0.478 (resp. 0.56) on a void square, and 0.071 (resp. 0.125) on a square with crossed links. The correlation function of this observable is defined as usual as:

$$\begin{aligned} \mathcal{C}^8(\alpha, \beta, \gamma, \delta; i, j, k, l) &= \langle Q_{\alpha,\beta,\gamma,\delta} Q_{i,j,k,l} \rangle \\ &\quad - \langle Q_{\alpha,\beta,\gamma,\delta} \rangle \langle Q_{i,j,k,l} \rangle \end{aligned} \quad (7.3)$$

Its values are displayed in Table VI. One might notice the presence of non negligible correlations between void squares and the quasi absence between squares with crossed links. The short distance value of these correlations shows the limits of relevance of the variational description. As expected from the spectra, the checkerboard Heisenberg magnet is a Valence Bond Crystal.

VIII. CONCLUSION

The spin-1/2 checkerboard Heisenberg antiferromagnet is a Valence Bond Crystal with LRO in 4-spin $S=0$ plaquettes: it exhibits a large spin gap, a breaking of the translational symmetry, a doubling of the unit cell and long range correlations in singlets.

At variance with the kagomé antiferromagnet this system does not exhibit a singlet continuum but a clear gap in the singlet sector above the (quasi-)degenerate ground-state.

This system is a 2-dimensional analog of the dimerized phase of the $J_1 - J_2$ on a chain. It belongs to the same generic class as the Shastry-Sutherland model [26] and the $J_1 - J_2$ model [27-29] on the square lattice for $J_1 - J_2 \sim 0.5$. Dimer LRO has also been found on the $J_1 - J_2$ model on the honeycomb lattice [30]. In these last examples, the dimerized phases are found after destabilization of a classical collinear Néel ground-state by quantum fluctuations as predicted from $SU(N)$ or $Sp(N)$ approaches [31,32]. A common feature of all these magnets is a bipartite lattice. Such an underlying lattice is prob-

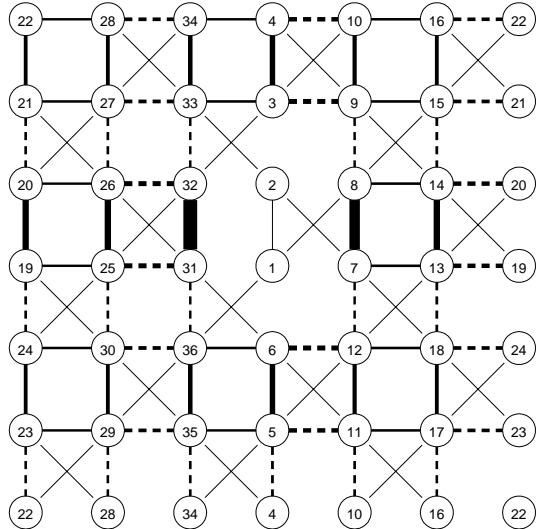


FIG. 10. Dimer-dimer correlations in the exact ground-state of the 36 sample (Eq. 7.1). The reference bond is the bond (1, 2). Positive (negative) correlations are drawn as full (dashed) lines. The thickness of the lines is a measure of the strength of the correlation. The diagonal lines show the position of the crossed links.

ably favorable for the establishment of LRO in dimer coverings.⁴

As shown in this paper the physics of the model in the singlet sector can essentially be captured in the restricted space of first neighbor coverings (FNSS). This explains why the Quantum Hard Core Dimer model on such a lattice gives essentially the same physics and phase diagram as the full Heisenberg model [24]. Nevertheless the renormalization by quantum fluctuations in the full Hilbert space is somewhat underestimated in the FNSS, and *a fortiori* in the Quantum Hard Core Dimer model.

This work also brings a new light on the discussion about the kagomé magnet. The local classical degeneracy of a model (present in any system with corner sharing units -as discussed in the introduction) is not a sufficient condition for the associated quantum model to exhibit a continuum of singlets and a residual entropy. Two pieces of information join to cast a doubt on the relationship

⁴ In each of these models the system is around the point of maximum classical frustration obtained for $z_2 J_2 = z_1 J_1 / 2$ (with z_i and J_i are respectively the coordinance and the coupling at distance i). In the $J_1 - J_2$ model on the square lattice there are still some controversies on the exact nature of the singlets with LRO (dimers or 4-spin plaquettes) [27-29], but no doubt about the belonging of this phase to the Valence Bond Crystal family.

between a classical continuous degeneracy and a kagomé like spectrum (type II Resonating Valence Bond Spin Liquid [33]):

- The checkerboard magnet has a continuum degeneracy in the classical limit but no continuum of singlets.
- The multi-spin exchange model on the triangular lattice (with an antiferromagnetic first neighbor coupling) has a continuum of singlets in the triplet gap but apparently no simple local continuous degeneracy in the classical limit.

Endly our results seem to indicate qualitative differences between planar and true 3-d pyrochlore (see section V above). In fact in the 3-d pyrochlore magnet, symmetric and antisymmetric spin singlets configurations on the tetrahedra are degenerate (as in the checker-board lattice), but there are no unique 4-spin $S=0$ configurations around the “voids” of the structure and the number of resonances on the loops encircling these voids is large. These quantum resonances are probably a very efficient mechanism to destabilize dimer LRO.

i, j	ex. g.-s.	Z w-f.	FNSS	i, j	ex. g.-s.	Z w-f.	FNSS
31,32	.56	.63	.55	7,13	.10	.25	.16
7,8	.43	.42	.39	19,25	.10	.25	.14
25,26	.26	.25	.21	7,12	-.10	-.25	-.15
13,14	.26	.25	.21	31,36	-.10	-.25	-.15
19,20	.25	.25	.21	13,18	-.11	-.25	-.16
6,5	.22	.25	.26	25,30	-.11	-.25	-.15
6,12	-.20	-.25	-.18	19,24	-.11	-.25	-.15
25,31	-.20	-.25	-.18	6,36	.10	.25	.16
13,19	-.18	-.25	-.18	12,18	.11	.25	.16
36,35	.18	.25	.18	24,30	.10	.25	.15
5,11	-.18	-.25	-.18	35,5	.10	.25	.15
4,10	-.18	-.25	-.18	11,17	.10	.25	.15
12,11	.17	.25	.19	29,23	.10	.25	.14
36,30	-.15	-.25	-.16	5,4	-.11	-.25	-.16
35,29	-.15	-.25	-.16	11,10	-.11	-.25	-.14
30,29	.15	.25	.17	35,34	-.11	-.25	-.14
17,23	-.15	-.25	-.16	17,16	-.11	-.25	-.14
18,17	.15	.25	.17	29,28	-.10	-.25	-.14
18,24	-.15	-.25	-.16	23,22	-.10	-.25	-.14
24,23	.15	.25	.16	34,4	.10	.25	.15
28,34	-.15	-.25	-.16	10,16	.10	.25	.15
16,22	-.15	-.25	-.16	28,22	.10	.25	.14

TABLE V. Dimer-dimer correlations $C^4(1, 2; i, j)$ (Eq. 7.1) in the $N = 36$ ground-state. The sites $1, 2, i, j$ are described in Fig. 10, the i, j points are enumerated in the first columns. This correlation has been measured in the exact ground-state wave function (second columns), in the variational Z state (third columns) and in the ground-state of Eq. 1 in the first neighbor singlet subspace (FNSS, fourth columns). All the values of these correlations between sites of Fig. 10 can be obtained from this table by a mirror symmetry through the bisector of bond $(1, 2)$.

-
- [1] A. P. Ramirez, *Annu. Rev. Mater. Sci* **24**, 453 (1994), and references therein.
- [2] A. Ramirez, *Handbook of magnetism* (PUBLISHER, ADDRESS, 2000).
- [3] A. Ramirez, G. P. Espinosa, and A. S. Cooper, *Phys. Rev. Lett.* **64**, 2070 (1990).
- [4] Y. Uemura *et al.*, *Phys. Rev. Lett.* **73**, 3306 (1994).
- [5] A. Keren *et al.*, *Phys. Rev. B* **53**, 6451 (1996).
- [6] P. Mendels *et al.*, *Phys. Rev. Lett.* **85**, 3496 (2000).
- [7] V. Elser, *Phys. Rev. Lett.* **62**, 2405 (1989).
- [8] J. Chalker, P. C. W. Holdsworth, and E. F. Shender, *Phys. Rev. Lett.* **68**, 855 (1992).
- [9] E. Shender, V. Cherepanov, P. Holdsworth, and A. Berlinsky, *Phys. Rev. Lett.* **70**, 3812 (1993).
- [10] R. Moessner and J. T. Chalker, *Phys. Rev. B* **58**, 12049 (1998).
- [11] S. Palmer and J. Chalker, *Phys. Rev. B* **62**, 488 (2000).
- [12] B. Canals, *cond-mat/0102233*.
- [13] A. Chubukov, *Phys. Rev. Lett.* **69**, 832 (1992).
- [14] B. Canals and C. Lacroix, *Phys. Rev. Lett.* **80**, 2933 (1998).
- [15] A. Koga and N. Kawakami, *Phys. Rev. B* **63**, 144432 (2001).
- [16] C. Waldtmann *et al.*, *Eur. Phys. J. B* **2**, 501 (1998).
- [17] P. Sindzingre *et al.*, *Phys. Rev. Lett.* **84**, 2953 (2000).
- [18] W. LiMing, G. Misguich, P. Sindzingre, and C. Lhuillier, *Phys. Rev. B* **62**, 6372,6376 (2000).
- [19] C. Lhuillier, P. Sindzingre, and J.-B. Fouet, *cond-mat/0009336*.
- [20] S. Palmer and J. Chalker, *cond-mat/0102447*.

$(1,31,32,2; 5,35,36, 6)$.172	$(7,1,2,8; 11, 5 ,6,12)$.073
$(1,31,32,2; 17,11,12,18)$.127	$(7,1,2,8; 23,17,18,24)$.009
$(1,31,32,2; 10, 4, 5,11)$	-.121	$(7,1,2,8; 16,10,11,17)$	-.006
$(1,31,32,2; 22,16,17,23)$	-.117	$(7,1,2,8; 28,22,23,29)$	-.004

TABLE VI. Plaquette-plaquette correlations $C^8(\alpha, \beta, \gamma, \delta; i, j, k, l)$ (Eq. 7.3) in the exact ground-state of the $N = 36$ sample. The sites are numbered as in Fig. 10. The left part of the table describes the correlations between void squares, the right part between squares with crossed links.

- [21] B. Bernu, P. Lecheminant, C. Lhuillier, and L. Pierre, Phys. Rev. B **50**, 10048 (1994).
- [22] E. H. Lieb and P. Schupp, Phys. Rev. Lett. **83**, 5362 (1999).
- [23] G. Misguich and C. Lhuillier, cond-mat/0002170 .
- [24] R. Moessner, O. Tchernyshyov, and S. L. Sondhi, cond-mat/0106286 .
- [25] M. Elhajal, B. Canals, and C. Lacroix, cond-mat/0104331 .
- [26] C. H. Chung, J. B. Marston, and S. Sachdev, cond-mat/0102222 .
- [27] L. Capriotti and S. Sorella, Phys. Rev. Lett. **84**, 3173 (2000).
- [28] O. P. Sushkov, J. Oitmaa, and Z. Weihong, Phys. Rev. B **63**, 104420 (2001).
- [29] M. S. .L. du Croo de Jongh, J. M. .J. van Leeuwen, and W. van Saarloos, Phys. Rev. B **62**, 14844 (2000).
- [30] J.-B. Fouet, P. Sindzingre, and C. Lhuillier, Eur. Phys. J. B **20**, 241 (2001).
- [31] N. Read and S. Sachdev, Phys. Rev. B **42**, 4568 (1990).
- [32] N. Read and S. Sachdev, Phys. Rev. Lett. **66**, 1773 (1991).
- [33] C. Lhuillier and G. Misguich, Cargese Lecture notes of the School “Trends in high magnetic field science” to be published in Springer Series. .